sustainability

MDPI

Article

Effect of Class C and Class F Fly Ash on Early-Age and Mature-Age Properties of Calcium Sulfoaluminate Cement Paste

Sukanta K. Mondal [1,2], Carrie Clinton [1,2], Hongyan Ma [3], Aditya Kumar [4] and Monday U. Okoronkwo [1,2,*]

[1] Sustainable Materials Laboratory (SusMatLab), Missouri University of Science and Technology, Rolla, MO 65409, USA
[2] Department of Chemical & Biochemical Engineering, Missouri University of Science and Technology, Rolla, MO 65409, USA
[3] Department of Civil, Architectural and Environmental Engineering, Missouri University of Science and Technology, Rolla, MO 65409, USA
[4] Department of Materials Science and Engineering, Missouri University of Science and Technology, Rolla, MO 65409, USA
* Correspondence: okoronkwom@mst.edu; Tel.: +1-573-341-4349

Abstract: To promote the sustainable development of eco-efficient calcium sulfoaluminate (CSA) cements through the partial replacement of the CSA clinker with supplementary cementitious waste products, the effects of coal fly ashes on the early-age and mature-age properties of a calcium sulfoaluminate (CSA)-based cement paste were investigated. The impacts of both Class C and Class F fly ashes on the rheological properties, hydration kinetics, and compressive strength development of CSA cement paste were studied. Rheology-based workability parameters, representing the rate of loss of flowability, the rate of hardening, and the placement limit, were characterized for the pastes prepared with fixed water-to-cement (w/c) and fixed water-to-binder (w/b) ratios. The results indicate a slight improvement in the workability of the CSA paste by fly ash addition at a fixed w/b ratio. The isothermal calorimetry studies show a higher heat of hydration for the Class C fly ash-modified systems compared to the Class F-modified systems. The results show that fly ash accelerates the hydration of the calcium sulfoaluminate cement pastes, chiefly due to the filler effects, rather than the pozzolanic effects. In general, ettringite is stabilized more by the addition of Class F fly ash than Class C fly ash. Both fly ashes reduced the 1-day compressive strength, but increased the 28-day strength of the CSA cement paste; meanwhile, the Class C modified pastes show a higher strength than Class F, which is attributed to the higher degree of reaction and potentially more cohesive binding C-S-H-based gels formed in the Class C fly ash modified systems. The results provide insights that support that fly ash can be employed to improve the performance of calcium sulfoaluminate cement pastes, while also enhancing cost effectiveness and sustainability.

Keywords: sulfoaluminate cement; fly ash; hydration; rheology; eco-efficient cement; sustainability of cements

Citation: Mondal, S.K.; Clinton, C.; Ma, H.; Kumar, A.; Okoronkwo, M.U. Effect of Class C and Class F Fly Ash on Early-Age and Mature-Age Properties of Calcium Sulfoaluminate Cement Paste. *Sustainability* **2023**, *15*, 2501. https://doi.org/10.3390/su15032501

Academic Editor: Ning Yuan

Received: 16 December 2022
Revised: 26 January 2023
Accepted: 27 January 2023
Published: 30 January 2023

1. Introduction

Calcium sulfoaluminate (CSA) cements are one of the most promising low-CO_2 sustainable alternatives to Portland Cements (PC) [1–3]. CSA cements feature a lower carbon footprint than PC, mainly because the raw material-derived CO_2 emission arising from the formation of the major CSA clinker phase, ye'elimite (C_4A_3S), is about a third of that arising from the formation of the major PC clinker phase, alite (C_3S) [4]. In addition, the lower clinkering temperature of 1250 °C used for CSA cement production leads to a lower fuel-derived CO_2 emission compared to PC, with a clinkering temperature of 1450 °C. Furthermore, the CSA clinker generally requires lower energy to grind. In addition to the reduced CO_2 emission and energy consumption, CSA cement features superior properties,

for example, high early-age strengths [5,6] and shrinkage minimization [7,8]. However, unanswered questions regarding durability have limited the adoption of CSA cements in mainstream construction applications in many countries [9]. Nevertheless, one of the significant limitations of the general use of CSA is, arguably, its high cost, which is about twice the cost of an equivalent bag of PC.

To make CSA cement greener and to reduce its cost, it can be blended with supplementary cementitious materials (SCMs), for example, fly ash and slag [10,11], silica fume [12], or limestone powder [13–15]. Expectedly, the addition of SCMs to cement will modify their properties; this is via SCMs' participation in the hydration reaction (e.g., like a pozzolan), via a filler effect, or via a combination of the two. The effects of fly ash and other SCMs in PC systems have been extensively studied [16–18], wherein fly ash in PC is known to serve both as a filler and as a pozzolan [16–21]. The pozzolanic effect enhances cement hydration via the reaction of the siliceous components of the fly ash with free portlandite to produce new hydration products (e.g., C-S-H gel), while the filler effect accelerates the hydration reaction via the additional nucleation sites for reaction product precipitation on the extra surfaces provided by the SCM particles [22]. Secondly, the filler effect is also attributed to the dilution effect of replacing cement with SCM, which increases the effective water/cement (w/c) ratio and results in an increased hydration of the cement. Given the generally low reactivity of fly ash, the filler effect is known to be the most dominant effect of fly ash at the early ages of cement hydration [17,19,20].

Unlike PC, limited studies have been devoted to understanding the effects of SCMs in CSA cement systems [10,23,24]. It is known that the pore solutions of CSA cement generally have a lower pH than that of PC at early hydration ages [1,25,26], which suggests that the dissolution of fly ash will be slower in CSA systems. In addition, contrary to the PC system, pozzolanic reactions are limited in the CSA cement system due to portlandite unavailability. However, for CSA cements containing belite and alite, C-S-H gel may form upon the dissolution of these calcium silicate clinker phases. This can potentially provide accessible calcium ions that may react with fly ash, leading to C-S-H gels with a decreased calcium/silica ratio [18,21]. Previous studies have shown that the addition of fly ash to CSA cement leads to an increase in the 28-day compressive strength by up to 6 MPa for CSA cement, substituted by up to 15% fly ash. Conversely, a higher replacement, above 15% fly ash, has been reported to lead to a decrease in the compressive strength [10,11]. It is also reported that fly ash may promote the early formation of ettringite in CSA cements [10,24], whereas the product of the fly ash reaction in the system (i.e., strätlingite) was detected after about half a year of hydration, suggesting that there was a minimal degree of fly ash reaction in the CSA system [10].

One of the most critical challenges that constrain the general applicability of CSA cement in conventional construction is its poor early-age workability. CSA cement paste is a shear-thickening material that features a rapid-changing rheological behavior [10]; as a result, chemical admixtures (e.g., retarders and dispersants) are frequently employed to control the rheology [27]. Moreover, mineral admixtures (e.g., fly ash, silica fume, and slag) have been reported to improve the rheological properties of CSA cement paste in a few studies [12,28]. The studies show different trends for different supplementary cementitious materials, for example, silica fume lowers the plastic viscosity but increases the yield stress, while fly ash and granulated blast furnace slightly reduce both the plastic viscosity and yield stress [12]. Similar effects of SCMs on cement paste rheology have been reported for PC systems [29–32], however, unlike the extensive studies available for PC systems, studies on the effects of fly ash on the early-age characteristics of CSA pastes are still limited.

To better understand the impact of fly ash on the early-age and mature-age properties of CSA cements, this study investigates the impacts of ASTM C618-compliant Class C and Class F on the rheology and hydration kinetics of belite-CSA cement pastes. ASTM C618 [33] specifies the chemical and physical characteristics of Type C and Fly ashes, suitable for use in cement and concrete. Class C fly ash is typically produced from burning lignite or subbituminous coal, and may also be produced from anthracite or bituminous coal, while

Class F fly ash is typically produced from burning anthracite or bituminous coal, but may also be produced from subbituminous coal and from lignite [33]. It is important to note that depending on the locality of a coal source, the coal combustion residue or fly ash may contain contaminants of significant environmental concern, including heavy metals [34,35] and radionuclides [36,37], which may require a proper ecological risk assessment.

The early-age properties of cement-based materials are the properties of the fresh paste, from mixing to about 3 days after setting (e.g., rheology, workability, the heat of hydration and set time); meanwhile, the mature-age properties are those hardened properties usually measured after 28 days of hydration (e.g., compressive strength, flexural strength, microstructure, and porosity). Both the early-age and mature-age properties are critical in determining the performance and durability of the final cement and concrete products. In this study, a time-dependent rheological method [38,39] is used to quantify the workability of the fly ash-dosed CSA cement pastes, while isothermal calorimetry is employed to characterize hydration kinetics. Thermodynamic modeling is employed to provide long-term phase assemblage insight, and a compressive strength test is used to investigate the mechanical performance. The findings improve the understanding of the fly ash interaction with CSA cement systems, and may be used to develop guidelines on the utilization of fly ash in the design of CSA cement-based concretes.

2. Materials and Methods

2.1. Materials

The belite calcium sulfoaluminate cement (CSAC) used in this study was received from Buzzi Unicem USA, while the ASTM C618-compliant Class C fly ash (FA-C) and Class F fly ash (FA-F), originating from the USA, were received from LafargeHolcim USA. The oxide compositions of the CSA cement and fly ashes, analyzed by energy-dispersive x-ray fluorescence spectroscopy (EDXRF; Oxford X-Supreme 8000, Hitachi High-Tech Analytical Science, Abingdon, Oxfordshire, UK), are shown in Table 1. The powder X-ray diffraction (XRD) pattern of the fly ashes and CSAC, obtained by a PANalytical X'Pert Pro multipurpose diffractometer with a 2θ configuration using CuKα (λ = 1.540 Å) radiation, is presented in Figure 1a. The mineral compositions of the materials were quantified by the Rietveld refinement of the x-ray diffraction pattern [40], using corundum as an internal standard. The CSA cement is composed of 52% ye'elimite, 21% belite, and 27% anhydrite ($\%_{mass}$basis). The FA-C is composed of 23% crystalline phases, and 77% amorphous phases, whereas FA-F contains 8% crystalline phases and 92% amorphous phases. An analytical-grade citric acid (CA) additive (citric acid monohydrate, 99.5%) was used as a set retarder. The mean particle sizes of CSAC, FA-C, and FA-F samples were 2.85 µm (D_{50}: 2.26 µm), 2.24 µm (D_{50}: 1.40 µm) and 4.35 µm (D_{50}: 2.15 µm), respectively. The particle size distribution of the CSAC and fly ash samples are shown in Figure 1b.

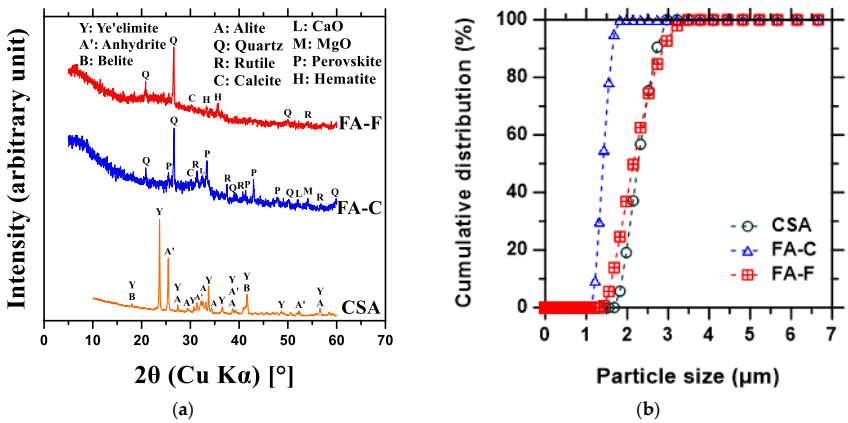

Figure 1. (**a**) XRD pattern of commercial calcium sulfoaluminate cement (CSAC), Class C and Class F fly ashes (FA-C, and FA-F), and (**b**) Particle size distribution of CSA cement and fly ash samples used in this study. The XRD patterns have been shifted vertically; the intensity axis is marked as arbitrary units.

Table 1. Oxide composition of CSA cement and fly ashes (%mass).

Species	MgO	CaO	Al_2O_3	SiO_2	P_2O_5	SO_3	$Na_2O + K_2O$	TiO_2	Mn_2O_3	Fe_2O_3	LOI
CSAC [a]	0.94	48.85	20.94	11.61	0.48	11.49	0.34	0.53	0.09	2.96	1.65
FA-C [b]	5.22	32.13	16.64	32.31	1.46	1.74	1.47	1.40	0.03	6.07	1.16
FA-F [c]	1.51	6.04	18.88	56.50	0.73	1.21	3.08	0.75	0.05	10.11	1.06

[a] CSAC = Calcium sulfoaluminate cement; [b] FA-C = Class C Fly ash; [c] FA-F = Class F Fly ash.

2.2. Mixing Protocol

Twelve CSAC paste mix designs were prepared with six different dosages of FA-C and FA-F (0%, 1%, 3%, 5%, 10%, and 15% dry mass of cement) for the rheology study at a fixed water-to-CSA cement (w/c) of 0.5 (mass basis). To regulate (retard) the hydration rate, a fixed 2% citric acid was used. The proportion of the chemical admixtures was kept constant in all the pastes, while the dosage of fly ash was varied. Grade II deionized water was used in preparing the cement pastes. A second set of pastes was prepared with a fixed water-to-binder (w/b) = 0.5 (mass basis) to help explicate the effects at fixed w/c versus w/b. The water content in the chemical admixtures was accounted for as part of the total water.

The target mixture proportions of solids (CSA cement, fly ash, and citric acid powder) were first homogenized by handshaking before mixing with water to prepare the pastes. For the rheology study, 10 g of CSA cement was used, and the mixture was mixed in a 250 mL plastic beaker with a four-blade overhead stirrer (RW 20 Digital, IKA, Wilmington, NC, USA) for one minute at 1000 rpm. The mixed slurry was immediately loaded into the rheometer for the measurements. For isothermal calorimetry tests, similarly, mixed liquids were added to the mixed solids in a glass vial, and the manual mixing of the pastes continued for one minute. Then, the sample vial containing the obtained paste was lowered into the micro reaction calorimeter for analysis.

2.3. Parallel Plate Rheometry

The development of yield stress in the fresh cementitious pastes was measured as a function of time with a hybrid rheometer (DHR-2, TA Instruments, New Castle, DE, USA). The rheometer was equipped with 40 mm in diameter crosshatched top and bottom parallel plates. The cement pastes were contained in a fixed geometry gap of 1000 μm between the top and bottom plates. The temperature during the experiment was maintained at 25 °C. During measurement, a solvent trap filled with deionized water was used to maintain a constant humidity around the pastes.

The rheology measurements were started immediately after 5 min, from the time of the mixed solid's contact with the mixing water. The yield stress measurement by the stress growth method was used. The pastes were first pre-sheared for 30 s, followed by a 30 s rest, and then sheared at a very low fixed shear rate of 0.01 s^{-1} for 180 s to collect the static yield stress data. The shear stress at which the paste began to flow plastically during the fixed shear rate 0.01 s^{-1} was used to determine the "yield stress", as illustrated in Figure 2. The peak shear stress is a realistic approximation of the static yield stress [41,42]. The above measurement steps were repeated at intervals of 3 min on the same sample to track the time-dependent evolution of the yield stress of the CSAC+FA pastes until setting, or when the pastes could no longer be sheared by the rheometer or stress $\geq$ 15,000 Pa. Figure 2a displays a representative flow curve at a shear rate of 0.01 s^{-1} for a paste showing the determination of yield stress; meanwhile, Figure 2b shows a typical time-dependent yield stress evolution curve for concrete systems, showing two linear regimes with slopes m_1 and m_2, representing the rate of loss of flowability (or plasticity retention) and the rate of hardening, respectively [38,39]. The time, t_p, which marks the point of transition from flowability regime to rapid hardening regime, represents the placement time; i.e., the time at which the rapid loss of flowability sets in as the paste accelerates to setting,

such that at t_p, the mixture is unsuitable to be placed but remains finishable [39]. These rheological parameters were analyzed to examine the influence of fly ash on the CSAC paste workability. It is worth noting that similar curves to the one shown in Figure 2b can be produced by measuring the time-dependent dynamic yield stress or the viscosity evolution [38]; however, the present study focuses on static yield for simplicity and its relevance on placement, and the 3D printing of cement paste [43–45]. The described methodology has been applied to Portland cement and CSA cement systems in previous studies [38,39], and was found self-consistent for assessing the rheological parameters with a relative standard error $\leq 5\%$.

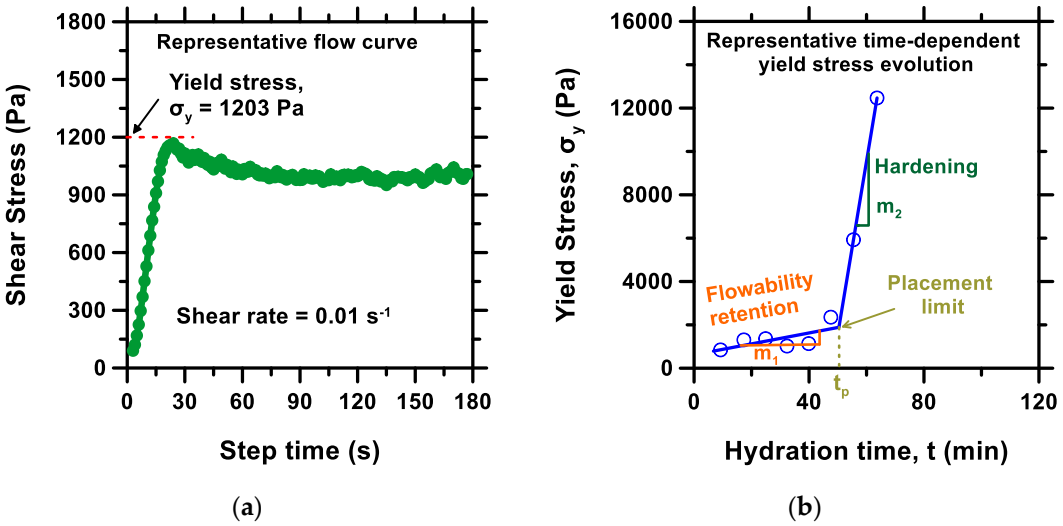

Figure 2. (**a**) Representative flow curve for a paste showing how yield stress (σ_y) was determined, (**b**) representative time-dependent yield stress evolution of CSAC+FA paste, showing the flowability retention regime with slope m_1, the placement limit t_p, and the hardening regime with slope m_2.

2.4. Calorimetry

To investigate the hydration kinetics of the fly ash-modified CSAC pastes, isothermal calorimetry was conducted for selected CSAC+FA pastes mixtures, used for the rheology studies. The mixtures containing 0%, 3%, and 15% FA dosages were studied. The heat evolution from the hydration of the CSAC+FA systems was monitored for 24 h, at a constant temperature of 25 ± 0.001 °C, and of 1.0 bar, using a THT µRC Peltier-based temperature-controlled isothermal micro reaction calorimeter (Thermal Hazard Technology, Bletchley, Milton Keynes, UK). A 1.5 mL glass vial with a standard polypyridene cap was used to load the samples into the microcalorimeter. The THT micro reaction calorimeter was helpful in this study since it is capable of monitoring heat evolution at a high resolution (5 µW) with a dynamic range of 5 µW–600 mW. The reference cell was provisioned with an inert reference sample (equivalent water) vial, with equivalent heat capacity as the paste sample to reduce noise and decrease the undesirable transient effects [46]. All the isothermal tests were started after 4.5 min of mixing the solid components with the liquids. The calorimetry data were correlated with the rheology data to provide some insights into the mechanisms.

2.5. Phase Assemblage Study

The mineralogy of the hydrated pastes was examined as a function of time by X-ray powder diffraction (XRD), using the PANalytical X'Pert Pro MultiPurpose Diffractometer (Philips Analytical, Netherland) to understand the effect of fly ash addition on the hydration product phase evolution. The diffractometer utilized CuKα radiation (wavelength λ = 1.540 Å) with a 2θ goniometer configuration. The samples were continuously scanned from 5° to 90° 2θ at a step size of 0.026° 2θ.

2.6. Thermodynamic Simulation

To investigate the potential long-term effects of the fly ashes on the hydrated phase assemblage in the CSAC pastes, a geochemical modeling package, GEM-Selektor v.3 (GEMS3) [47], based on the principle of Gibbs Energy Minimization, was used to simulate the hydration as a function of the amount of fly ash reacted, similar to related studies [48,49]. The thermodynamic properties of the relevant cement phases were taken from the built-in GEMS3 default database [50–52], and the published cement databases (CEMDATA18) [53]. The effects of solution non-ideality resulting from the presence of dissolved compounds were accounted for with the Truesdell–Jones form of the extended Debye–Hückel model [54].

2.7. Compressive Strength Tests

To evaluate the evolution of the mechanical properties, the compressive strength of the selected CSA cement pastes with and without fly ash modification was studied. The same mix proportions (Section 2.2, w/c = 0.5) were maintained in the preparation of 1-inch cubes. The ASTM C 305, ASTM C 109, and ASTM C 511-19 standards were followed for preparing and storing the cubes. The cubes were cured in a Perfa-Cure concrete curing box maintaining $\geq$ 95% humidity and a curing temperature of 23 $\pm$ 2 °C. A 200,000 lb servo-controlled Tinius Olsen universal compression machine with a data acquisition PC workstation was used for the compressive strength measurement. A load rate of 200 lb/s was maintained for every test. The compressive strength was obtained as the mean of three independent measurements.

3. Results and Discussion

This section may be divided by subheadings. It should provide a concise and precise description of the experimental results, their interpretation, as well as the experimental conclusions that can be drawn.

3.1. Effects of Fly Ash on the Rheological Properties

The time-dependent evolution of yield stress for the twelve investigated mixtures is presented in Figure 3a–d as a function of hydration time, showing the effect of the dosage rates of the different fly ashes. As expected, the curves feature two linear regimes, wherein the slopes of both regimes increased with the increasing dosage of fly ash. At fixed w/c (Figure 3a,b), the time of transition from the slow rising to the steep rising regime decreased with the increasing dosage of fly ash. These trends are a typical indication of a gradual loss of flowability, followed by a rapid acceleration to setting or hardening [39,55], which agrees with the rheology trends in previous studies of fly ash-blended CSAC systems with a fixed water-to-cement (w/c) ratio [10]. Conversely, at a fixed w/b (Figure 3c,d), the time of transition from the slow rising to the steep rising regime increases (shifts to the right) with the addition of fly ash, wherein a small difference is observed for the two fly ash types. In general, there are two potential causes of the observed rheology trend for the fly ash-modified cement pastes, namely, an increase in the hydration reaction due to pozzolanic effects, or due to the filler effect of the added fly ash at a fixed w/c ratio. Both processes lead to an increase in the hydration reaction and the precipitation of hydration products, resulting in an increased solid content and local structuring in the paste. Hence, high shear stress is required to sufficiently deform the material and cause it to flow due to the local structuring. On the other hand, when the w/b is fixed, the effective water increases with the addition of fly ash due to the lower water demand of fly ash compared to CSA cement powder, causing a slightly better rheology behavior (lesser slope of the two linear regimes).

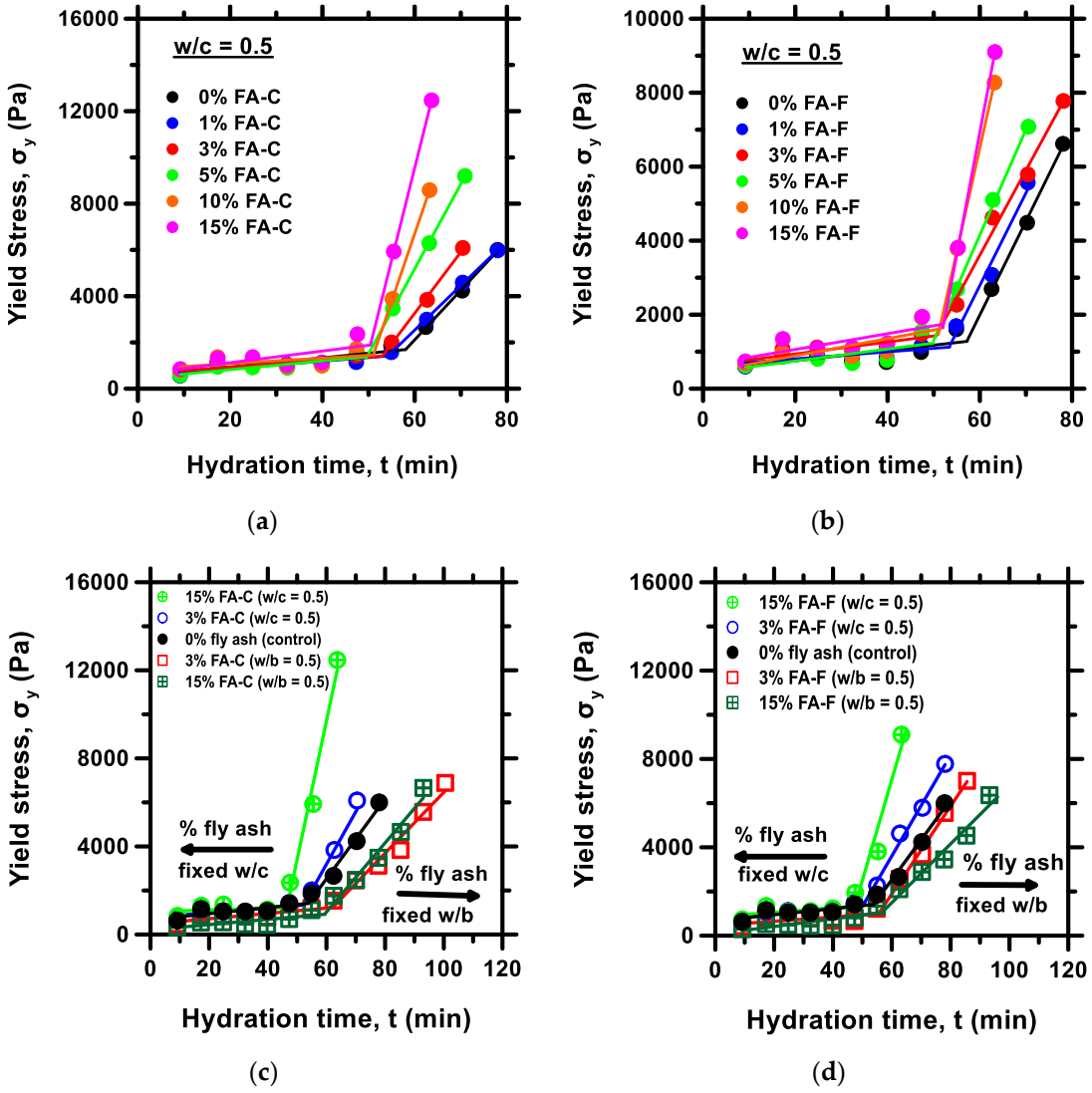

Figure 3. Time-dependent yield stress evolution: (**a**) Class C fly ash-dosed CSA pastes at fixed w/c = 0.5, (**b**) Class F fly ash-dosed CSA pastes at fixed w/c = 0.5, (**c**) Comparison of data for fixed w/c = 0.5 vs. fixed w/b = 0.5 for Class C fly ash-dosed pastes, and (**d**) Comparison of data from fixed w/c = 0.5 vs. fixed w/b = 0.5 for Class F fly ash-dosed pastes.

In a conventional PC paste, the pore solution features a higher pH (>12.5) and Ca^{2+} saturation than the dissolving clinker phases. This leads to the precipitation of free portlandite that readily reacts with the glass contents of SCMs (e.g., fly ash) pozzolanically, and yields additional C-S-H and other cement hydrate phases [56]. Contrary to the PC system, there is little or no pozzolanic effect of fly ash in the CSA cement, mainly because of the lower pH and non-availability of free Ca^{2+} in the CSA cement pore system. However, the CSAC used in this study contains calcium silicates (belite), which enhance the precipitation of the C-S-H gel that can potentially provide accessible Ca for a reaction with the fly ash particles. However, given the low reactivity of fly ash, coupled with the short rheology data acquisition time of under 2 h, it is unlikely that any reactive influence of fly ash has set in. Hence, the observed acceleration and yield stress growth, (i.e., hardening) in current CSAC systems would be mainly attributed to the solid content increase and the filler effect of the fly ashes [10,22,57–59].

To help elucidate the specific effects of the fly ash types and dosage, as described in the previous section (Figure 2b), the slopes of the two regimes, m_1 and m_2, representing the rate of loss of flowability and rate of hardening, respectively, and the placement time,

t_p, representing the point of transition from flowability regime to rapid hardening regime, were determined for the curves shown in Figure 3. The values are presented in Figure 4a–f, showing the evolution of m_1, m_2, and t_p as a function of the fly ash types and dosages at fixed w/c and fixed w/b. The overall trends are essentially similar for both the Class C and F fly ashes.

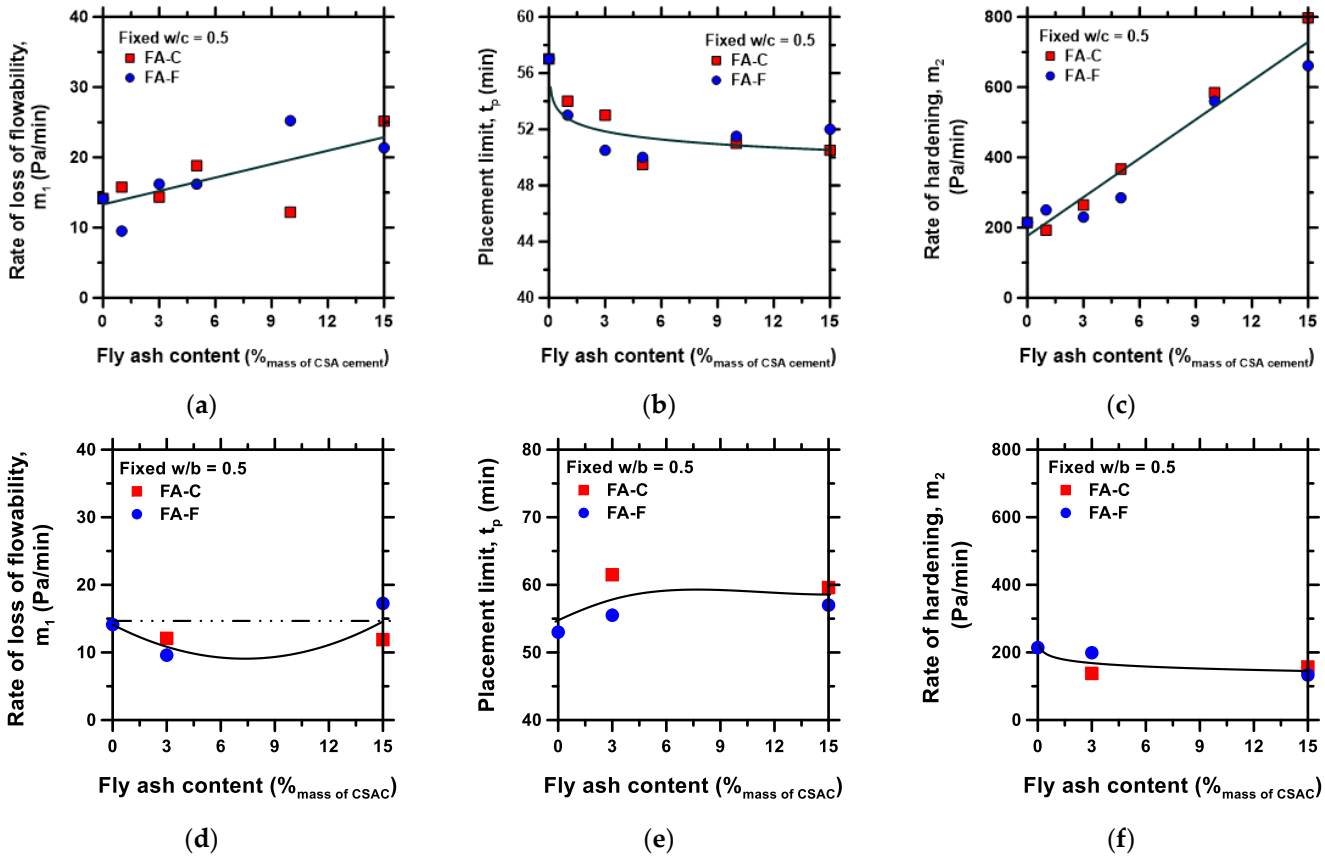

Figure 4. The evolution of the Rate of loss of flowability m_1, Placement time t_p, and Hardening rate m_2, at (**a**–**c**) at fixed w/c of 0.5; and (**d**–**f**) at fixed w/b of 0.5 for cement pastes with varying fly ash dosage. Fitting lines are for visual guides.

As is visible in Figure 4a, the slope m_1, which represents the rate of loss of flowability at a constant w/c, increases with the increasing content of both fly ash types, albeit with a small slope value and poor linearity. This suggests that the replacement of the CSAC with fly ash does not 'drastically' reduce the flowability of the paste at a constant w/c. The corresponding data at constant w/b (Figure 4d) clearly shows a drop in the m_1 followed by a rise back to an average value at 15% fly ash, similar to the value obtained for the control paste (with 0% fly ash). This indicates that fly ash improves the early-age flowability of the paste in agreement with previous studies [12,28], especially at dosages below 15% fly ash.

In addition, Figure 4b shows that the placement limit, t_p, decreases monotonically with increasing fly ash content at constant w/c. The trend observed for the t_p is expected because the filler effect of the fly ash accelerates the hydration reaction at an early age, leading to more solid hydration product formation, and local structuring of the paste, hence the shortening of the flowability regime and a reduction in the placement time (or the rheology set time) of the CSA+FA pastes. The t_p values initially decreases exponentially with an increasing dosage of fly ash and then decays into a plateau after about a 5% fly ash dosage of both fly ash types. These indicate that there is a threshold where the additional fly ash content does not significantly change the t_p parameters. The opposite, but less intense trend, is seen at constant w/b (Figure 4e), where the addition of fly ash led to an increase in t_p, indicating a slightly prolonged initial set [39], attributed to the dilution effect [12,30].

The hardening rate (m_2), shows a linear increase with the increasing fly ash content (Figure 4c) at a constant w/c, similar to, but stronger than the trends observed for m_1. Among the three rheology-based workability parameters, m_2 shows the strongest correlation with the fly ash dosages, with the trendline R^2 value of 0.95 for the pastes with a constant w/c. A high m_2 value suggests a paste that would be more suitable for 3D printing [60,61], while the opposite is the case for self-consolidating concrete or pastes for pumping applications. Corresponding data at a fixed w/b ratio show a downward trend, indicating a deceleration of the hardening rate with fly ash addition. However, the trend plateaus after about 3–5% fly ash, suggesting that a threshold exists where additional fly ash content may not significantly change the m_2 parameter at constant w/b. Previous studies have also found that the effects of fly ash on some properties of CSAC pastes are more significant at low dosages, and in some cases, a higher dosage may lead to a trend turnaround; these include the reported effects on compressive strength [10,11]. These findings could provide important guidelines on blended CSAC mix proportioning for specific purposes. Overall, it can be deduced that, due to the low water demand of fly ash compared to CSAC, the effects of fly ash at a fixed water-to-binder (w/b) ratio tend toward the retention of paste workability, while the opposite is the case at fixed w/c ratio.

Although the described early-age rheological behavior of the pastes can inform some aspects of reaction kinetics for optimizing the workability of the CSAC+FA pastes, no clear contrast is revealed regarding the action of Class C vs. Class F fly ash, despite the obvious difference in their chemistry (e.g., the high Ca content of Class C). Some differences are envisaged to exist in the interaction of the two types of fly ashes with the CSAC system. Hence, to provide more insight into the underlying mechanisms, this area is pursued to understand the impacts of both fly ash variations on the hydration kinetics and the hydrate phase assemblage in the following sections.

3.2. Effects on Hydration Kinetics

The hydration kinetics of selected pastes with fly ash dosages of 0%, 3%, and 15% were studied by isothermal calorimetry. The purpose of the isothermal calorimetry was to investigate the heat release profiles at the early age, elucidate the characteristics relatable to the rheological behavior of the pastes, understand the effects of the fly ash types, and help provide insights on the underlying mechanisms. Figure 5a,b shows the time-dependent heat flow curve and the cumulative heat generation for a 24 h hydration time of FA-C-dosed CSAC pastes at fixed w/c = 0.5, and Figure 5c,d shows similar data for FA-F-dosed pastes. Additionally, the data for CSA paste with no added admixture, i.e., no retarder, no superplasticizer, and no fly ash (labeled as "Neat CSA") are shown included in Figure 5's graphs. As seen, the acceleration peak is almost uncaptured in the neat CSAC used in this study, due to the rapid reaction (Figure 5a,c); however, the added retarder and dispersant helped to regulate the hydration and allow for the investigation of the chemical process. In addition, the cumulative heat of the "Neat CSA" cement after 24 h of hydration is clearly above all the other samples (0% to 15% FA-C and FA-F) containing retarder and superplasticizer, as described in the materials and methods.

As shown in Figure 5a,b, the heat flow slightly increased with the increasing FA-C content (at constant w/c), featuring a small rise in the amplitude of the induction shoulder, and an increase in the height of the acceleration peak and the slope of the acceleration regime. The shape and position of the heat flow are essentially similar but slightly shifted to the right for the 3% FA-C and to the left for the 15% FA-C. The 24 h cumulative heat release also increased with an increase in the fly ash content (Figure 5b). The heat flow profile of the FA-F-dosed pastes (Figure 5c) also shows an increase in the induction shoulder, and the acceleration peak and slope, but the peak position is slightly drifted to the left for the 3% and to the right for the 15% FA-F; meanwhile, the 24 h cumulative heat release shows very little difference between the 0%, 3% and 15% FA-F dosages (Figure 5d). Considering the uncertainties, the overall heat of the hydration profile agrees with the rheology data, suggesting an increase in the hydration rate with the increasing fly ash content at the early

hours of hydration, due to a higher effective water with increasing fly ash content. In the case of FA-F-dosed pastes, the effects on the heat of hydration are smaller and are not noticeable at 24 h of hydration; however, the heat release is apparently higher for FA-C-dosed pastes, and the effect of 15% FA-C is still noticeable at 24 h of cumulative heat release. Figure 6a presents the 24 h cumulative heat release as a function of fly ash type and dosage at constant w/c, showing no significant change for FA-F dosages; however, a noticeable rise is observed with the increasing dosage of FA-C. These results suggest that the effect of FA-F is mostly a minimal filler effect, while additional reactive effects may be involved in the case of FA-C. This observation is not surprising, since the high Ca content of FA-C will facilitate a reactive interaction that will yield new phases, such as x-ray amorphous C-S-H gel and monosulfate.

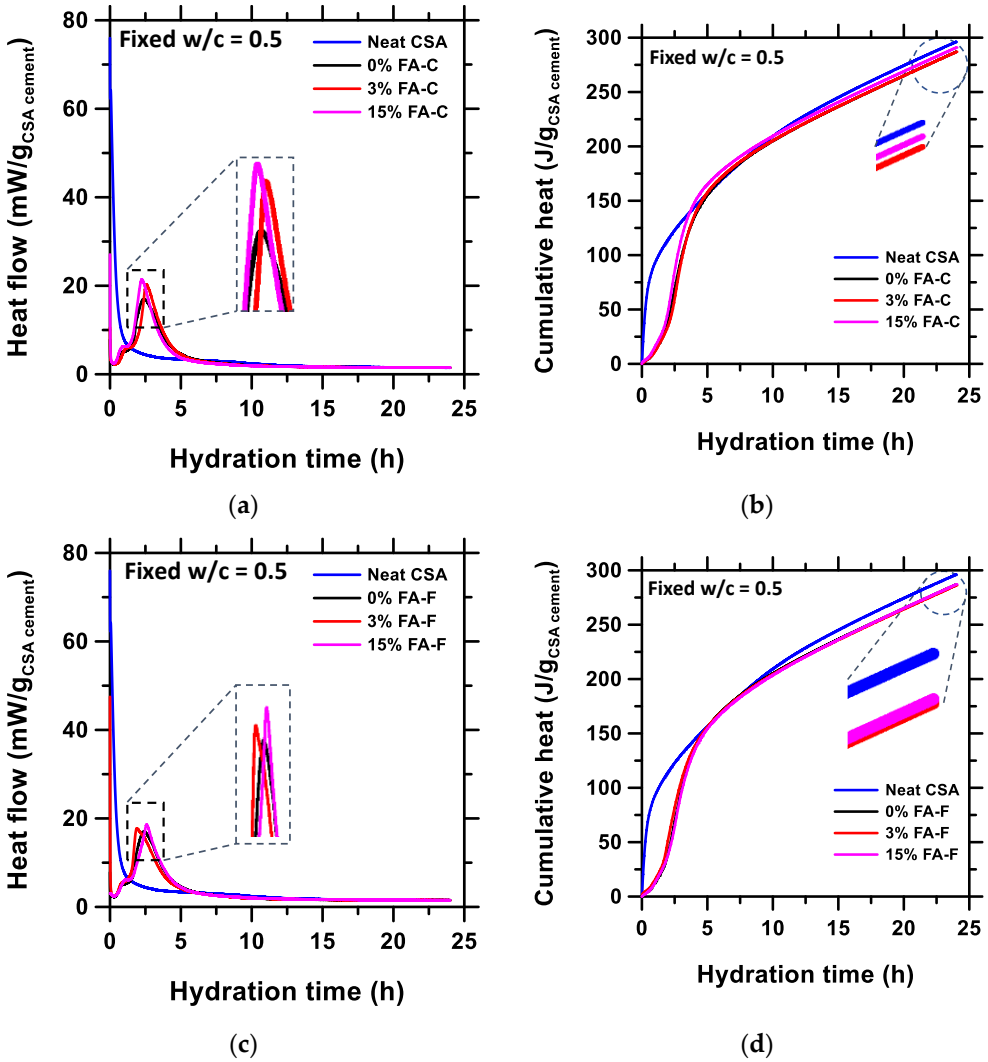

Figure 5. Isothermal calorimetry-based time-dependent (**a**) heat flow of [CSAC+FA-C] pastes, (**b**) cumulative heat released of [CSAC+FA-C] pastes, (**c**) heat flow of [CSAC+FA-F] pastes, (**d**) cumulative heat released of [CSAC+FA-F] pastes. "Neat CSA" represents paste with no added admixture. All pastes are for constant w/c = 0.5. Due to overlap of data points, some curves are shielded.

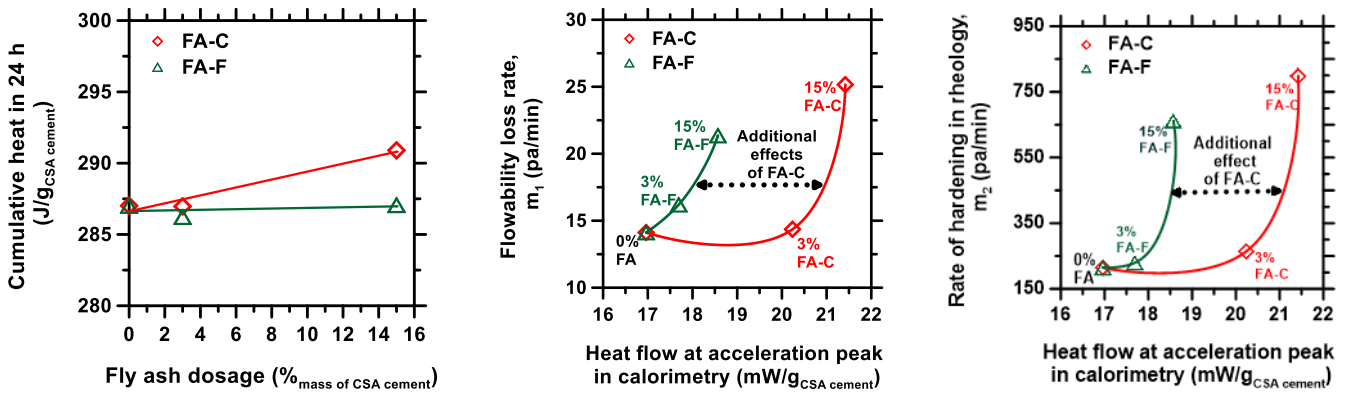

(**a**) (**b**) (**c**)

Figure 6. Relationship between rheological parameter and calorimetry data for two different fly ash-dosed CSA cement pastes; (**a**) 24 h cumulative heat released as a function of fly ash dosages, (**b**) flowability loss rates vs. heat flow at acceleration peaks, (**c**) rate of hardening vs. heat flow at acceleration peaks. Fitting lines are for visual guides.

Figure 6b,c show the correlation of the rheology-based loss of flowability (m_1) and hardening rate (m_2), with the heat flow at the acceleration peak for both fly ash types at constant w/c, respectively. The figures clearly show the dominance of the workability parameters over the rate of heat release from the hydration. Given that the rheology behavior and flow dynamics of materials are particle-interaction driven, it is indicative that the effects of the fly ashes are dominated by particle-driven filler effects and less reactive pozzolanic effects. However, a difference is noted between the FA-C and FA-F curves, as the curve is shifted to a higher rate of heat release for FA-C. Thus, while both fly ashes provide filler effects, it appears that FA-C releases more heat; this can be due to (i) the finer particle size of the FA-C (2.24 µm) compared to FA-F (4.35 µm), or (ii) due to the additional heat from exothermic dissolution and the reaction of the Ca-rich FA-C with cement particles to form new phases, such as x-ray amorphous C-S-H gel and monosulfate. To better understand the contribution of the latter, the mineral phase assemblage of the paste is examined in Section 3.3.

Figure 7 shows a comparison of the data at fixed w/c with corresponding data at fixed w/b. As seen in Figure 7a, there is a decrease in the cumulative heat release at 3% fly ash, followed by an increase at the 15% fly ash dose. This trend agrees with the rheology data, m_2 (Figure 4d) at constant w/b, suggesting a slight suppression of the hydration rate at the early age with fly ash addition, due to an initial soak-up of the water by fly ash; however, as the dosage of fly ash increases, the effective water content becomes significantly improved, leading to a higher overall hydration rate due to more water availability [56]. However, contrary to the observation by Martin et al. [56], the heat flow at the acceleration peak in the present study is generally reduced with fly ash addition at constant w/b compared to the paste with 0% fly ash (Figure 7b,c), suggesting potentially more reaction occurring in the system without fly ash. The difference in the current study compared to the observation by Martin et al. [56] can be attributed to the compositional differences in the CSA cement systems. In general, the higher the heat flow at the acceleration peak, the higher the flowability loss (m_1) and the hardening rate (m_2) for both fly ash types. As seen in Figure 7b,c, the fly ash-dosed pastes with fixed w/c = 0.5 are clearly clustered at higher acceleration heat flow peak and higher (m_1) and (m_2), while the pastes with fixed w/b = 0.5 are clustered at lower values of those parameters, relative to the control with zero fly ash. These observations expectedly support more reaction leading to a higher yield stress build-up.

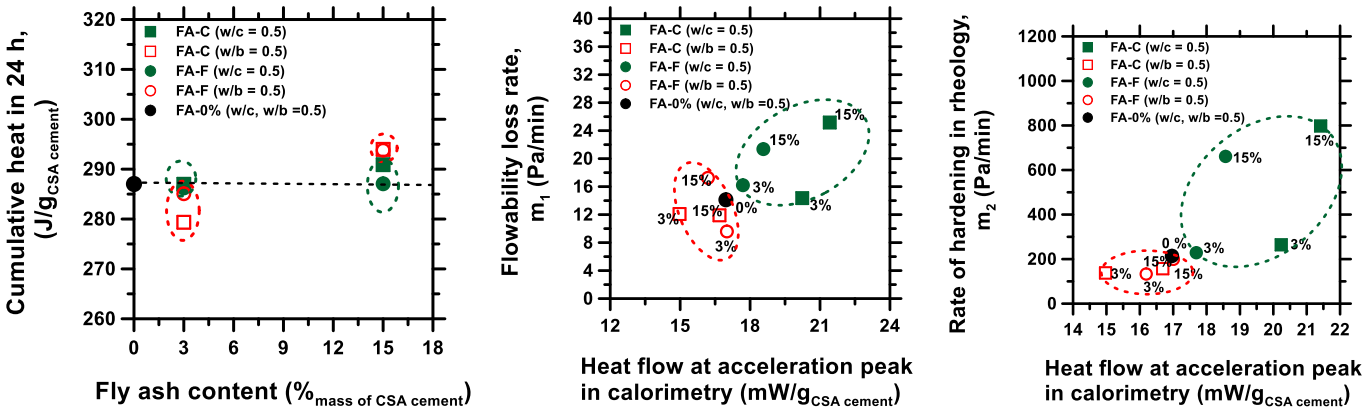

Figure 7. Comparing the effect of fixed w/c versus fixed w/b: (**a**) 24 h cumulative heat released as a function of fly ash dosages, (**b**) flowability loss rates vs. heat flow at acceleration peaks, (**c**) rate of hardening vs. heat flow at acceleration peaks.

3.3. Effects on Phase Assemblages

The pastes containing 0% and 15% fly ashes were characterized by X-ray powder diffraction after 16 h, 28 days, and 52 days of hydration, in order to understand the effect of fly ash on the early-age and mature-age evolution of hydrate phase assemblage. This is to understand the effect of fly ash on both the early- and later-age evolution of the hydrate-phase assemblage. This is to investigate whether the fly ashes have significant reactive effects on the CSA cement system, given that the studies presented in the preceding sections suggest that the effects of the fly ash addition were mostly filler effects, rather than reactive effects (such as pozzolanic). Hence, the highest fly ash dosage of 15%, where there is a higher probability of observing a reactive effect, was investigated in comparison with the control (0% fly ash). Figure 8 displays the XRD patterns, showing essentially a similar phase assemblage, dominated by crystalline ettringite in all the pastes. The quantitative estimate of the amount of ettringite by Rietveld refinement is presented in Figure 9a, showing a slightly higher amount of crystalline ettringite in the control paste at 28–52 days, compared to the system containing fly ash. Slightly more ettringite is formed in the FA-F-dosed pastes than in the FA-C-dosed pastes. It is believed that the crystallization of ettringite is favored most in the FA-F-dosed pastes, due to the higher destabilization of monosulfate with increasing siliceous contents and the concomitant stabilization of ettringite (and potentially x-ray amorphous strätlingite and katoite may form [62–64] after sufficient time has passed), in agreement with previous studies [56,62,65]. Conversely, due to the high calcium supply from FA-C, monosulfates, being stable in a Ca-rich environment [66], tend to compete with ettringite in the system [64]. Consequently, ettringite is slightly suppressed within the early age hydration of the FA-C-dosed pastes. However, it is expected that, long term, the ettringite–monosulfate balance will tilt to favor the thermodynamically more stable ettringite at a normal temperature (~25 °C) [67].

The reaction of fly ash (if it does react) with CSA cement is expected to modify the phase assemblage and thus generate new phases, although some of the products may be X-ray amorphous. To investigate the effect of the potential reaction of the added fly ash, the 15% fly ash pastes were simulated with the GEMS as a function of the percentage of the fly ash reacted, from 0 to 50% of the total added fly ash, while assuming a full reaction of the CSA cement component. Figure 9b shows the evolution of ettringite with the increasing reaction of fly ash. As seen in Figure 9b, the amount of ettringite formed increases linearly, wherein the ettringite formed in the FA-F-dosed paste is consistently higher than the amount formed in the FA-C-dosed paste. Thus, ettringite formation is enhanced more in class F fly ash-modified paste, in agreement with the experimental data.

How this observation affects the strength development is presented in the following section.

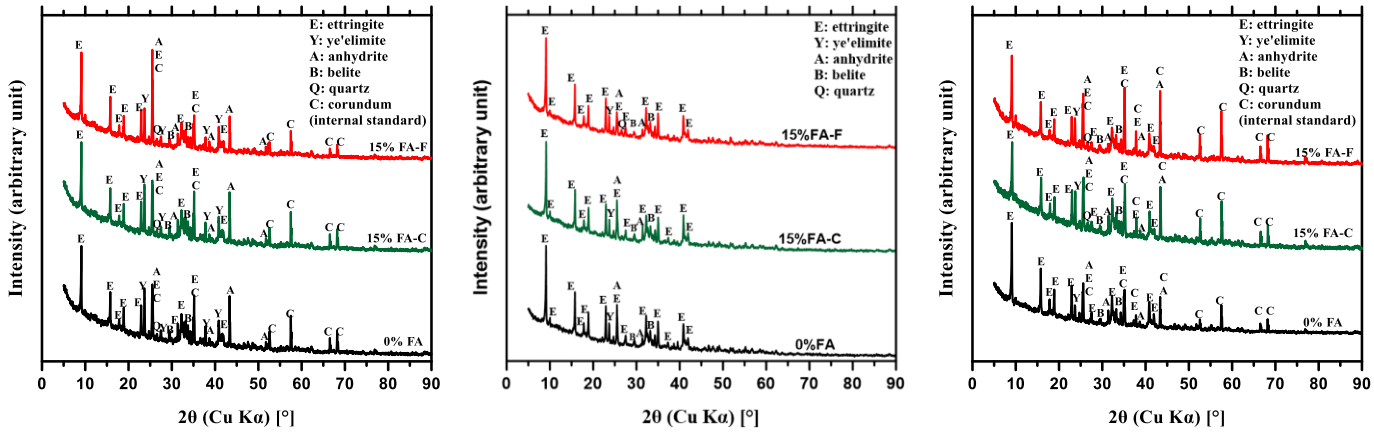

Figure 8. The XRD pattern of the CSAC+FA pastes after (**a**) 16 h, (**b**) 28 days, and (**c**) 52 days of hydration. Detected corundum in the 16 h and 52-day samples is an internal standard to aid the quantitative XRD analysis of amorphous phases; this was was found negligible compared to ettringite.

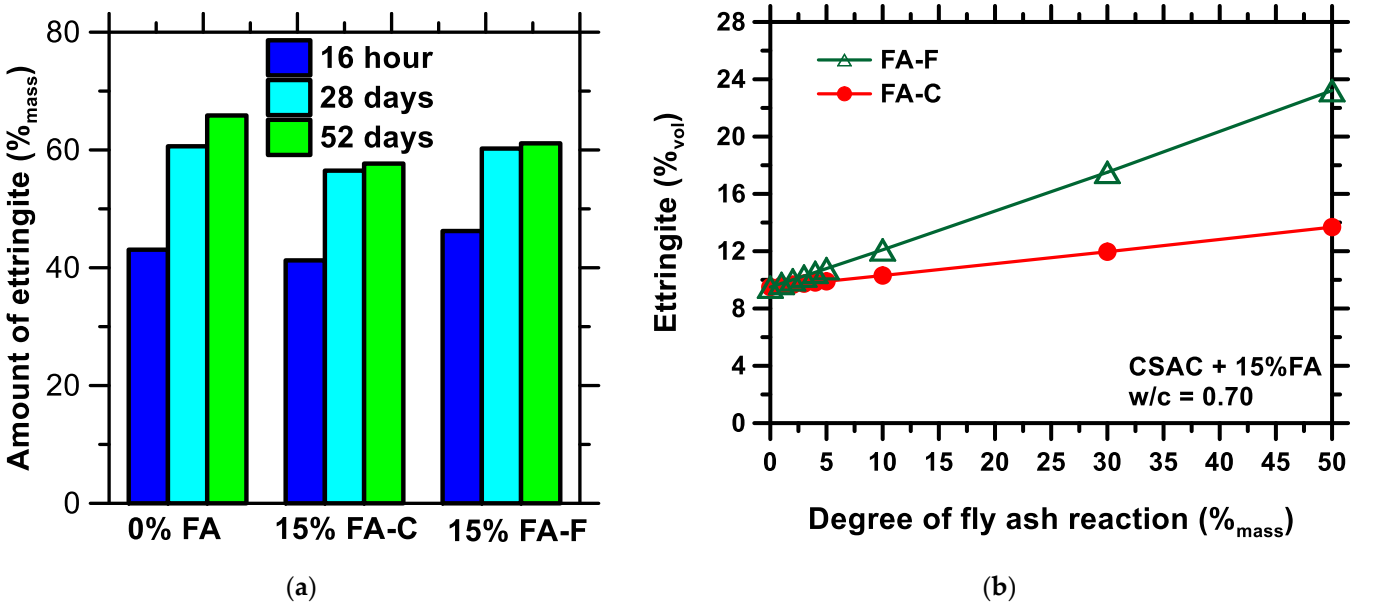

Figure 9. (**a**) Quantitative XRD estimation of amounts of ettringite formed in pastes containing 0% and 15% fly ash type C and F, and cured for 16 h, 28 days, and 52 days; (**b**) Evolution of ettringite with increasing degree of fly ash reaction, calculated using the GEMS software.

3.4. Effects on Compressive Strength

The 1-day and 28-day compressive strength data of CSA cement paste containing 0% and 15% class C and F fly ash types are shown in Figure 10a. The results indicate that the addition of fly ash lowered the 1-day compressive strength but increased the 28-day strength. High early-age buildability and strength are the most important properties of CSA cements. This result indicates that fly ash addition to CSA cement may provide a minimal improvement to early-age past buildability (i.e., increase in yield stress as described in Section 3.1), but it does not benefit the early-age mechanical strength development, as seen in Figure 10a. However, fly ash may improve the mature-age compressive strength, as seen in Figure 10a, in agreement with previous studies [68,69]. Thus, due to the slow interaction of fly ash with the CSA system, there is a lower cohesion of the particles with

the hydration products of CSA cement at the early-age; hence, the strength development is less rapid at day 1 for the fly ash-dosed paste compared to the control. However, as curing is prolonged, and the fly ash particles gradually react, interact and bond with the CSA hydration phases, the compressive strength of the fly ash-dosed pastes eventually increases, exceeding that of the control paste. Given that fly ash C reactivity was slightly higher, as seen from the calorimetry studies, the compressive strength is also higher than that of the class F fly ash at 28 days. However, the differences are minimal, which indicates that there are similarities in the physical and chemical properties of both classes of fly ash. Ettringite is known as the major contributor to the strength of CSA cements, but the amount formed in FA-C-dosed pastes was slightly lower than the amount formed in the FA-F pastes, leading to the consideration that other factors play an influential role, e.g., porosity evolution and the degree of fly ash reaction in both fly ash systems. To understand the effects of the fly ash reaction on the porosity evolution, the systems containing 15% fly ash were simulated with the GEMS as a function of the percentage of the fly ash reacted, from 0 to 50% of the total added fly ash; this assumes a full reaction of the CSA cement component. Figure 10b displays the calculated porosity as a function of the % of fly ash reacted. As seen in Figure 10b, as the percentage of fly ash reacted increases, the porosity of the fly ash-dosed pastes decreased gradually, which may, among other factors, contribute to the observed strength increase at the later curing age of 28 days. The porosity of the FA-F-dosed pastes is consistently lower with an increasing reaction rate, but the strength is lower; this suggests that the degree of the reaction of the FA-C may have been higher (in agreement with calorimetry data) to produce the higher strength recorded for FA-C, compared to the FA-F-dosed pastes at similar ages.

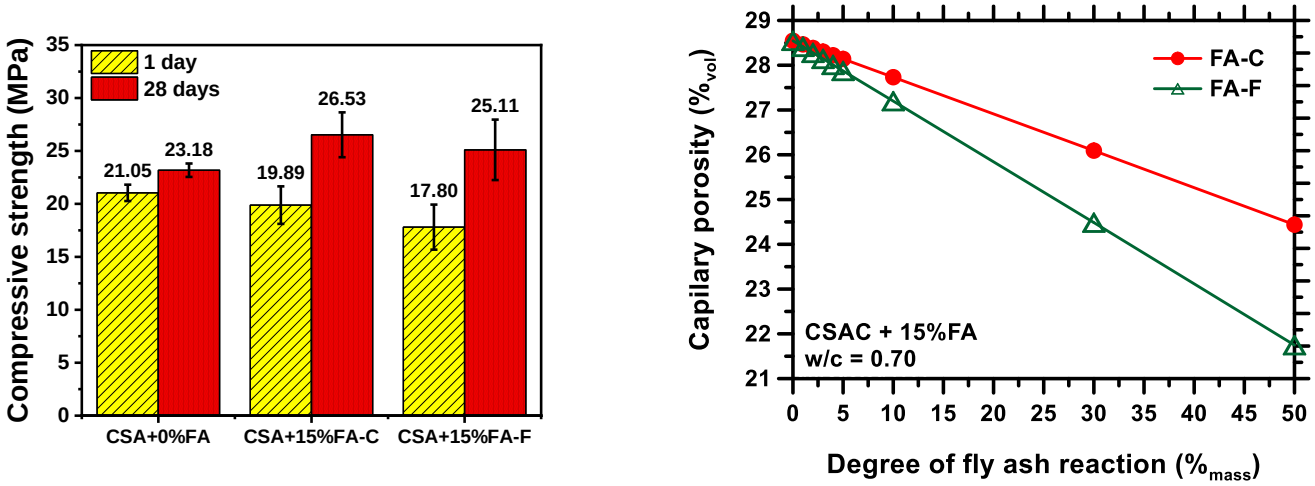

(**a**) (**b**)

Figure 10. (**a**) Compressive strength of control CSA and 15% fly ash-dosed CSA cement pastes. All the pastes were prepared with similar chemical admixtures; (**b**) Simulated porosity of CSAC + 15% fly ash as a function of the degree of fly ash reaction up to 50% of added fly ash, assuming a full reaction of the CSA cement component of the blended paste.

In summary, the results of the 15% fly ash-dosed pastes display an average 28-day increase in strength of 11% for both fly ash types, in comparison with the control CSA cement with 0% fly ash (Figure 10a). Assuming the average cost of CSA cement is ~ USD 225/ton and fly ash is ~ USD 20/ton, a 15% fly ash substitution represents a ~13% reduction in the cost of the cement material. Thus, the fly ash addition not only enables the improvement of the mature-age properties, but may also enhance the cost-effectiveness, eco-efficiency, and sustainability of calcium sulfoaluminate cement.

4. Conclusions

The effects of Class C and F fly ashes on the early-age and mature-age properties of a belite calcium sulfoaluminate (CSA) cement paste were studied. A rheology-based method was employed to investigate the effects on workability parameters, specifically, the rate of loss of flowability (m_1), the evolution of placement limit (t_p), and the hardening rate (m_2). Both fly ash types show a similar influence on these workability parameters, wherein the m_1 and m_2 increase with the increasing dosage of both fly ashes, while t_p decays monotonically with increases in the content of both Class C and F fly ashes at a fixed w/c ratio; conversely, an opposite but less intense trend is obtained at a fixed w/b ratio. Overall, fly ash addition slightly improves the early-age workability of the CSA cement paste at constant w/b. The hydration kinetics were also investigated by isothermal calorimetry, which revealed a slightly higher hydration heat release for the Class C fly ash-dosed pastes compared to the Class F fly ash, suggesting a slightly higher reaction in class C fly ash pastes. An experimental and simulated equilibrium mineral phase assemblage indicates that the low-Ca Class F fly ash enhanced the volume of the ettringite formed, compared to high-Ca Class C fly ash-dosed pastes. Compressive strength studies show that both fly ashes decreased the 1-day compressive strength, but slightly improved the 28-day compressive strength of the CSA cement paste; meanwhile, the fly ash C-dosed pastes outperformed the class F-dosed pastes in strength development. The findings provide valuable insights into the effects of the different fly ash types that can help advance mix design selection and fly ash utilization in CSA cement systems for improved cost-effectiveness and performance.

Author Contributions: Conceptualization, M.U.O.; Methodology, S.K.M. and M.U.O.; Data curation, S.K.M.; Formal analysis, S.K.M., C.C. and M.U.O.; Funding acquisition, M.U.O.; Investigation, S.K.M. and C.C.; Project administration, M.U.O.; Resources, M.U.O.; Supervision, M.U.O.; Validation, H.M., A.K. and M.U.O.; Writing—original draft, S.K.M.; Writing—review and editing, S.K.M., H.M., A.K. and M.U.O. All authors have read and agreed to the published version of the manuscript.

Funding: This work has been supported by the National Science Foundation through CMMI: 1932690.

Institutional Review Board Statement: Not applicable.

Informed Consent Statement: Not applicable.

Data Availability Statement: Not applicable.

Acknowledgments: Funding support from National Science Foundation (NSF CMMI: 1932690) is acknowledged. The contents of this paper reflect the views and opinions of the authors, who are responsible for the accuracy of the data presented herein. The authors are thankful to GCP Applied Technologies, USA, and Buzzi Unicem, USA, for providing test materials. The research was conducted in the Sustainable Materials Laboratory (SusMatLab) with instrumental support from the Materials Research Center (MRC) at Missouri S&T. All supports that enable the operation of SusMatLab and MRC are acknowledged.

Conflicts of Interest: The authors declare no conflict of interest.

References

1. Juenger, M.; Winnefeld, F.; Provis, J.L.; Ideker, J. Advances in Alternative Cementitious Binders. *Cem. Concr. Res.* **2011**, *41*, 1232–1243. [CrossRef]
2. Coppola, L.; Coffetti, D.; Crotti, E. An Holistic Approach to a Sustainable Future in Concrete Construction. *IOP Conf. Ser. Mater. Sci. Eng.* **2018**, *442*, 012024. [CrossRef]
3. Gartner, E. Industrially Interesting Approaches to "Low-CO_2" Cements. *Cem. Concr. Res.* **2004**, *34*, 1489–1498. [CrossRef]
4. Li, G.; Walenta, G.; Gartner, E. Formation and Hydration of Low-CO_2 Cements Based on Belite, Calcium Sulfoaluminate and Calcium Aluminoferrite. In Proceedings of the 12th ICCC, Montreal, QC, Canada, 8–13 July 2007; pp. 9–12.
5. Odler, I. *Special Inorganic Cements*; CRC Press: Boca Raton, FL, USA, 2000; ISBN 1-4822-7194-X.
6. Glasser, F.P.; Zhang, L. High-Performance Cement Matrices Based on Calcium Sulfoaluminate–Belite Compositions. *Cem. Concr. Res.* **2001**, *31*, 1881–1886. [CrossRef]
7. Zhou, Q.; Milestone, N.; Hayes, M. An Alternative to Portland Cement for Waste Encapsulation—The Calcium Sulfoaluminate Cement System. *J. Hazard. Mater.* **2006**, *136*, 120–129. [CrossRef]

8. Coumes, C.C.D.; Courtois, S.; Peysson, S.; Ambroise, J.; Pera, J. Calcium Sulfoaluminate Cement Blended with OPC: A Potential Binder to Encapsulate Low-Level Radioactive Slurries of Complex Chemistry. *Cem. Concr. Res.* **2009**, *39*, 740–747. [CrossRef]
9. Tan, B.; Okoronkwo, M.U.; Kumar, A.; Ma, H. Durability of Calcium Sulfoaluminate Cement Concrete. *J. Zhejiang Univ. Sci. A* **2020**, *21*, 118–128. [CrossRef]
10. García-Maté, M.; De la Torre, A.; León-Reina, L.; Aranda, M.; Santacruz, I. Hydration Studies of Calcium Sulfoaluminate Cements Blended with Fly Ash. *Cem. Concr. Res.* **2013**, *54*, 12–20. [CrossRef]
11. Živica, V. Properties of Blended Sulfoaluminate Belite Cement. *Constr. Build. Mater.* **2000**, *14*, 433–437. [CrossRef]
12. Ke, G.; Zhang, J.; Xie, S.; Pei, T. Rheological Behavior of Calcium Sulfoaluminate Cement Paste with Supplementary Cementitious Materials. *Constr. Build. Mater.* **2020**, *243*, 118234. [CrossRef]
13. Martin, L.H.; Winnefeld, F.; Müller, C.J.; Lothenbach, B. Contribution of Limestone to the Hydration of Calcium Sulfoaluminate Cement. *Cem. Concr. Compos.* **2015**, *62*, 204–211. [CrossRef]
14. Hargis, C.W.; Telesca, A.; Monteiro, P.J. Calcium Sulfoaluminate (Ye'elimite) Hydration in the Presence of Gypsum, Calcite, and Vaterite. *Cem. Concr. Res.* **2014**, *65*, 15–20. [CrossRef]
15. Pelletier-Chaignat, L.; Winnefeld, F.; Lothenbach, B.; Müller, C.J. Beneficial Use of Limestone Filler with Calcium Sulphoaluminate Cement. *Constr. Build. Mater.* **2012**, *26*, 619–627. [CrossRef]
16. De Weerdt, K.; Haha, M.B.; Le Saout, G.; Kjellsen, K.O.; Justnes, H.; Lothenbach, B. Hydration Mechanisms of Ternary Portland Cements Containing Limestone Powder and Fly Ash. *Cem. Concr. Res.* **2011**, *41*, 279–291. [CrossRef]
17. Bouzoubaa, N.; Min-Hong, Z.; Malhotra, V.; Golden, D.M. Blended Fly Ash Cements—A Review. *ACI Mater. J.* **1999**, *96*, 641–650.
18. Deschner, F.; Winnefeld, F.; Lothenbach, B.; Seufert, S.; Schwesig, P.; Dittrich, S.; Goetz-Neunhoeffer, F.; Neubauer, J. Hydration of Portland Cement with High Replacement by Siliceous Fly Ash. *Cem. Concr. Res.* **2012**, *42*, 1389–1400. [CrossRef]
19. Fraay, A.; Bijen, J.; De Haan, Y. The Reaction of Fly Ash in Concrete a Critical Examination. *Cem. Concr. Res.* **1989**, *19*, 235–246. [CrossRef]
20. Baert, G.; Hoste, S.; De Schutter, G.; De Belie, N. Reactivity of Fly Ash in Cement Paste Studied by Means of Thermogravimetry and Isothermal Calorimetry. *J. Therm. Anal. Calorim.* **2008**, *94*, 485–492. [CrossRef]
21. Lothenbach, B.; Scrivener, K.; Hooton, R. Supplementary Cementitious Materials. *Cem. Concr. Res.* **2011**, *41*, 1244–1256. [CrossRef]
22. Gutteridge, W.A.; Dalziel, J.A. Filler Cement: The Effect of the Secondary Component on the Hydration of Portland Cement: Part I. A Fine Non-Hydraulic Filler. *Cem. Concr. Res.* **1990**, *20*, 778–782. [CrossRef]
23. Ma, B.; Li, X.; Shen, X.; Mao, Y.; Huang, H. Enhancing the Addition of Fly Ash from Thermal Power Plants in Activated High Belite Sulfoaluminate Cement. *Constr. Build. Mater.* **2014**, *52*, 261–266. [CrossRef]
24. Ioannou, S.; Reig, L.; Paine, K.; Quillin, K. Properties of a Ternary Calcium Sulfoaluminate–Calcium Sulfate–Fly Ash Cement. *Cem. Concr. Res.* **2014**, *56*, 75–83. [CrossRef]
25. Andac, M.; Glasser, F. Pore Solution Composition of Calcium Sulfoaluminate Cement. *Adv. Cem. Res.* **1999**, *11*, 23–26. [CrossRef]
26. Winnefeld, F.; Lothenbach, B. Hydration of Calcium Sulfoaluminate Cements—Experimental Findings and Thermodynamic Modelling. *Cem. Concr. Res.* **2010**, *40*, 1239–1247. [CrossRef]
27. Li, G.; Zhang, J.; Song, Z.; Shi, C.; Zhang, A. Improvement of Workability and Early Strength of Calcium Sulphoaluminate Cement at Various Temperature by Chemical Admixtures. *Constr. Build. Mater.* **2018**, *160*, 427–439. [CrossRef]
28. Ke, G.; Zhang, J. Effects of Retarding Admixture, Superplasticizer and Supplementary Cementitious Material on the Rheology and Mechanical Properties of High Strength Calcium Sulfoaluminate Cement Paste. *J. Adv. Concr. Technol.* **2020**, *18*, 17–26. [CrossRef]
29. Ahari, R.S.; Erdem, T.K.; Ramyar, K. Effect of Various Supplementary Cementitious Materials on Rheological Properties of Self-Consolidating Concrete. *Constr. Build. Mater.* **2015**, *75*, 89–98. [CrossRef]
30. Park, C.; Noh, M.; Park, T. Rheological Properties of Cementitious Materials Containing Mineral Admixtures. *Cem. Concr. Res.* **2005**, *35*, 842–849. [CrossRef]
31. Correa-Yepes, J.A.; Rojas-Reyes, N.; Tobón, J.I. Effect of Fly Ash and Silica Fume on Rheology, Compressive Strength and Self-Compacting in Cement Mixtures. *DYNA* **2018**, *85*, 59–68. [CrossRef]
32. Shanahan, N.; Tran, V.; Williams, A.; Zayed, A. Effect of SCM Combinations on Paste Rheology and Its Relationship to Particle Characteristics of the Mixture. *Constr. Build. Mater.* **2016**, *123*, 745–753. [CrossRef]
33. *ASTM C618*; Standard Specification for Coal Fly Ash and Raw or Calcined Natural Pozzolan for Use in Concrete. ASTM International: West Conshohocken, PA, USA, 2022; p. 4. Available online: https://www.astm.org/c0618-22.html (accessed on 10 January 2023).
34. Altıkulaç, A.; Turhan, Ş.; Kurnaz, A.; Gören, E.; Duran, C.; Hançerlioğulları, A.; Uğur, F.A. Assessment of the Enrichment of Heavy Metals in Coal and Its Combustion Residues. *ACS Omega* **2022**, *7*, 21239–21245. [CrossRef] [PubMed]
35. Chaudhary, S.; Banerjee, D.K. Speciation of Some Heavy Metals in Coal Fly Ash. *Chem. Speciat. Bioavailab.* **2007**, *19*, 95–102. [CrossRef]
36. Temuujin, J.; Surenjav, E.; Ruescher, C.H.; Vahlbruch, J. Processing and Uses of Fly Ash Addressing Radioactivity (Critical Review). *Chemosphere* **2019**, *216*, 866–882. [CrossRef] [PubMed]
37. Tang, Y.; Pan, J.; Li, B.; Zhao, S.; Zhang, L. Residual and Ecological Risk Assessment of Heavy Metals in Fly Ash from Co-Combustion of Excess Sludge and Coal. *Sci. Rep.* **2021**, *11*, 2499. [CrossRef]

38. Mondal, S.K.; Welz, A.; Clinton, C.; Khayat, K.; Kumar, A.; Okoronkwo, M.U. Quantifying the Workability of Calcium Sulfoaluminate Cement Paste Using Time-Dependent Rheology. *Materials* **2022**, *15*, 5775. [CrossRef]
39. Okoronkwo, M.U.; Falzone, G.; Wada, A.; Franke, W.; Neithalath, N.; Sant, G. Rheology-Based Protocol to Establish Admixture Compatibility in Dense Cementitious Suspensions. *J. Mater. Civ. Eng.* **2018**, *30*, 04018122. [CrossRef]
40. Rietveld, H.M. A Profile Refinement Method for Nuclear and Magnetic Structures. *J. Appl. Crystallogr.* **1969**, *2*, 65–71. [CrossRef]
41. Nguyen, Q.; Boger, D. Measuring the Flow Properties of Yield Stress Fluids. *Annu. Rev. Fluid Mech.* **1992**, *24*, 47–88. [CrossRef]
42. Sant, G.; Ferraris, C.F.; Weiss, J. Rheological Properties of Cement Pastes: A Discussion of Structure Formation and Mechanical Property Development. *Cem. Concr. Res.* **2008**, *38*, 1286–1296. [CrossRef]
43. Chen, M.; Li, L.; Wang, J.; Huang, Y.; Wang, S.; Zhao, P.; Lu, L.; Cheng, X. Rheological Parameters and Building Time of 3D Printing Sulphoaluminate Cement Paste Modified by Retarder and Diatomite. *Constr. Build. Mater.* **2020**, *234*, 117391. [CrossRef]
44. Yuan, Q.; Li, Z.; Zhou, D.; Huang, T.; Huang, H.; Jiao, D.; Shi, C. A Feasible Method for Measuring the Buildability of Fresh 3D Printing Mortar. *Constr. Build. Mater.* **2019**, *227*, 116600. [CrossRef]
45. Roussel, N. Rheological Requirements for Printable Concretes. *Cem. Concr. Res.* **2018**, *112*, 76–85. [CrossRef]
46. Linderoth, O.; Wadsö, L.; Jansen, D. Long-Term Cement Hydration Studies with Isothermal Calorimetry. *Cem. Concr. Res.* **2021**, *141*, 106344. [CrossRef]
47. Kulik, D.A.; Wagner, T.; Dmytrieva, S.V.; Kosakowski, G.; Hingerl, F.F.; Chudnenko, K.V.; Berner, U.R. GEM-Selektor Geochemical Modeling Package: Revised Algorithm and GEMS3K Numerical Kernel for Coupled Simulation Codes. *Comput. Geosci.* **2013**, *17*, 1–24. [CrossRef]
48. Okoronkwo, M.U.; Balonis, M.; Katz, L.; Juenger, M.; Sant, G. A Thermodynamics-Based Approach for Examining the Suitability of Cementitious Formulations for Solidifying and Stabilizing Coal-Combustion Wastes. *J. Environ. Manag.* **2018**, *217*, 278–287. [CrossRef]
49. Mondal, S.K.; Welz, A.; Rownaghi, A.; Wang, B.; Ma, H.; Rezaei, F.; Kumar, A.; Okoronkwo, M.U. Investigating the Microstructure of High-Calcium Fly Ash-Based Alkali-Activated Material for Aqueous Zn Sorption. *Environ. Res.* **2021**, *198*, 110484. [CrossRef] [PubMed]
50. Hummel, W.; Berner, U.; Curti, E.; Pearson, F.J.; Thoenen, T. *Nagra/PSI Chemical Thermodynamic Data Base 01/01*; Nagra: Wettingen, Switzerland, 2002.
51. Johnson, J.W.; Oelkers, E.H.; Helgeson, H.C. SUPCRT92: A Software Package for Calculating the Standard Molal Thermodynamic Properties of Minerals, Gases, Aqueous Species, and Reactions from 1 to 5000 Bar and 0 to 1000 °C. *Comput. Geosci.* **1992**, *18*, 899–947. [CrossRef]
52. Thoenen, T.; Humel, W.; Berner, U. The PSI/Nagra Chemical Thermodynamic Database 12/07: Present Status and Future Developments. *Mineral. Mag.* **2013**, *77*, 2297–2370. [CrossRef]
53. Lothenbach, B.; Kulik, D.A.; Matschei, T.; Balonis, M.; Baquerizo, L.; Dilnesa, B.; Miron, G.D.; Myers, R.J. Cemdata18: A Chemical Thermodynamic Database for Hydrated Portland Cements and Alkali-Activated Materials. *Cem. Concr. Res.* **2019**, *115*, 472–506. [CrossRef]
54. Helgeson, H.C.; Brown, T.H.; Nigrini, A.; Jones, T.A. Calculation of Mass Transfer in Geochemical Processes Involving Aqueous Solutions. *Geochim. Cosmochim. Acta* **1970**, *34*, 569–592. [CrossRef]
55. Bentz, D.P.; Ferraris, C.F. Rheology and Setting of High Volume Fly Ash Mixtures. *Cem. Concr. Compos.* **2010**, *32*, 265–270. [CrossRef]
56. Martin, L.H.J.; Winnefeld, F.; Tschopp, E.; Müller, C.J.; Lothenbach, B. Influence of Fly Ash on the Hydration of Calcium Sulfoaluminate Cement. *Cem. Concr. Res.* **2017**, *95*, 152–163. [CrossRef]
57. Gutteridge, W.A.; Dalziel, J.A. Filler Cement: The Effect of the Secondary Component on the Hydration of Portland Cement: Part 2: Fine Hydraulic Binders. *Cem. Concr. Res.* **1990**, *20*, 853–861. [CrossRef]
58. Oey, T.; Kumar, A.; Bullard, J.W.; Neithalath, N.; Sant, G. The Filler Effect: The Influence of Filler Content and Surface Area on Cementitious Reaction Rates. *J. Am. Ceram. Soc.* **2013**, *96*, 1978–1990. [CrossRef]
59. Schöler, A.; Lothenbach, B.; Winnefeld, F.; Zajac, M. Hydration of Quaternary Portland Cement Blends Containing Blast-Furnace Slag, Siliceous Fly Ash and Limestone Powder. *Cem. Concr. Compos.* **2015**, *55*, 374–382. [CrossRef]
60. Chen, M.; Yang, L.; Zheng, Y.; Huang, Y.; Li, L.; Zhao, P.; Wang, S.; Lu, L.; Cheng, X. Yield Stress and Thixotropy Control of 3D-Printed Calcium Sulfoaluminate Cement Composites with Metakaolin Related to Structural Build-Up. *Constr. Build. Mater.* **2020**, *252*, 119090. [CrossRef]
61. Jones, S.Z.; Bentz, D.P.; Martys, N.S.; George, W.L.; Thomas, A. Rheological Control of 3D Printable Cement Paste and Mortars. In Proceedings of the First RILEM International Conference on Concrete and Digital Fabrication—Digital Concrete, Zurich, Switzerland, 10–12 September 2018; Wangler, T., Flatt, R.J., Eds.; Springer International Publishing: Cham, Switzerland, 2019; pp. 70–80.
62. Okoronkwo, M.U.; Glasser, F.P. Strätlingite: Compatibility with Sulfate and Carbonate Cement Phases. *Mater. Struct.* **2016**, *49*, 3569–3577. [CrossRef]
63. Okoronkwo, M.U.; Glasser, F.P. Stability of Strätlingite in the CASH System. *Mater. Struct.* **2016**, *49*, 4305–4318. [CrossRef]
64. Okoronkwo, M.U.; Glasser, F.P. Compatibility of Hydrogarnet, $Ca_3Al_2(SiO_4)x(OH)_4(3-x)$, with Sulfate and Carbonate-Bearing Cement Phases: 5–85 °C. *Cem. Concr. Res.* **2016**, *83*, 86–96. [CrossRef]
65. Okoronkwo, M.U. Phase Development in Cement Hydrate Systems. Ph.D.Thesis, University of Aberdeen, Aberdeen, Scotland, UK, 2014.
66. Matschei, T.; Lothenbach, B.; Glasser, F.P. The AFm Phase in Portland Cement. *Cem. Concr. Res.* **2007**, *37*, 118–130. [CrossRef]

67. Matschei, T.; Lothenbach, B.; Glasser, F.P. Thermodynamic Properties of Portland Cement Hydrates in the System $CaO–Al_2O_3–SiO_2–CaSO_4–CaCO_3–H_2O$. *Cem. Concr. Res.* **2007**, *37*, 1379–1410. [CrossRef]
68. Berry, E.; Malhotra, V.M. Fly Ash for Use in Concrete—A Critical Review. *ACI J. Proc.* **1980**, *77*, 59–73. [CrossRef]
69. Mirza, J.; Mirza, M.; Roy, V.; Saleh, K. Basic Rheological and Mechanical Properties of High-Volume Fly Ash Grouts. *Constr. Build. Mater.* **2002**, *16*, 353–363. [CrossRef]